Proceedings of SPIE's 6th Annual International Symposium on Smart Structures and Materials, 1-5 March, 1999, Newport Beach, CA. Paper No. 3669-33

Scaling Laws of Microactuators and Potential Applications of Electroactive Polymers in MEMS

Chang Liu[a], and Y. Bar-Cohen[b]

[a]University of Illinois at Urbana-Champaign, Urbana, IL
[b]Jet Propulsion Laboratory, Pasadena, CA

ABSTRACT

Besides the scale factor that distinguishes the various spices fundamentally biological muscles changes little between species indicating a highly optimized system, Electroactive polymer actuators offer the closest resemblance to biological muscles however beside the large actuation displacement these materials are falling short with regards to the actuation force. As improved materials emerging it is becoming necessary to address key issues such as the need for effective electromechanical modeling and guiding parameters in scaling the actuators. In this paper, we will review the scaling laws for three major actuation mechanisms that are of relevance to micro electromechanical systems: electrostatic actuation, magnetic actuation, thermal bimetallic actuation, and piezoelectric actuation.

Keywords: MEMS, micro actuators, electroactive polymers, EAP

I. INTRODUCTION

In the past decade, MEMS technology has been advanced significantly and rapidly. MEMS is a vastly enabling technology that provide innovative system design concepts, fabrication methods, and use. The essence of MEMS is the integrated microfabrication technology, also called micromachining (1-7).

Major intrinsic advantages of MEMS, as compared with conventional electromechanical systems and sensors, include the following:

(1) **Miniaturization**: As a result of the photolithography process, MEMS systems can have extremely small features (on the order of micrometer are routinely achievable) and have well-controlled geometric properties. Characteristic length scale of MEMS components is in the range of 1 micrometer to 1 cm. The small size makes it possible to insert micro electromechanical systems into a variety of applications that were previous not possible or practical. For example, MEMS pressure sensors are being integrated with the automotive tires to provide on-line realtime monitoring of tire pressure (8). Micromachined drug delivery systems are being considered for use as implantable smart drug capsules (9), micro inertia sensors are being used for smart projectiles to automatically adjust the trajectory for gun jump and wind factors. Micromachined digital propulsion is finding applications in controlling the position of micro satellite (10). In these particular applications, the insertion of smart function was previously not possible with macroscopic devices.

(2) **Compact integration of comprehensive functionality**: Mechanical structures and active components are integrated with electronics (e.g. signal processing circuits), sensors (temperature, pH sensors, etc.), optics, fluid components (e.g. fluid channels, micro pumps, micro valves), and high performance chemical analytical systems (e.g. electrophoresis) to realize comprehensive functional integration in "smart" sensors and actuators. The level of electromechanical integration is not achievable through any other means.

(3) **Mass fabrication and repeatability of performance**: Because integrated fabrication processes do not involve direct manual modification and assembly, device fabrication can be extremely efficient and reliable even though the size of individual devices are so small that they can no longer be handled by human hands. The photolithography process enables individual components to have extremely uniform geometry and performance, a major advantages in contrast to hand assembled instruments;

II. ACTUATION METHODS

Electrostatic Actuation

The parallel plate capacitor (Fig. 1) is the most fundamental configuration of capacitive sensors. The definition of capacitance, C, is

$$C = \frac{Q}{V} \tag{1}$$

where Q is the stored charge, V is the electrostatic potential. The stored electrostatic energy is expressed as[1]

$$E = \frac{1}{2}CV^2 = \frac{1}{2}\frac{Q^2}{C}. \tag{2}$$

Neglecting the fringe electric field, the field lines are extended uniformly through the capacitor plates. According to Gauss's law, the magnitude of the electric field, E, is related to Q by

$$E = Q/\varepsilon A \tag{3}$$

Plug Eq. 3 into Eq. 1, we have

$$C = \frac{Q}{\frac{Q}{\varepsilon A}d} = \frac{\varepsilon A}{d}. \tag{4}$$

This is the fundamental expression for the capacitance. The magnitude of the capacitance is related to the distance and overlap area. It is also a function of the electric permitivity, ε, which is subject to influence by temperature, humidity, surface conditions, etc.

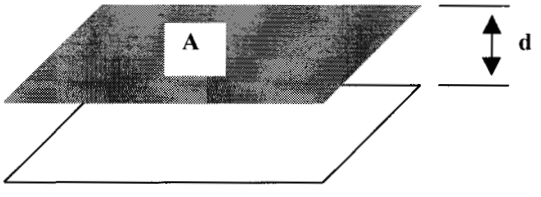

Fig. 1. A schematic diagram of a parallel plate capacitor.

[1] Energy is expressed as $E = \frac{1}{2}\int_v D \cdot EdV$ in general. Eq. 2 can be obtained by plugging in E=V/d.

Force in different directions can be generated. The magnitude of forces is expressed using a general equation

$$F = \frac{\partial E}{\partial x} = \frac{1}{2}\frac{\partial C}{\partial x}V^2 \tag{5}$$

whereas x is the coordinate of interest. For example, the force perpendicular to the plates (acting in the direction of thickness) can be expressed as

$$F = \frac{\partial E}{\partial d} = -\frac{1}{2}\frac{\varepsilon A}{d^2}V^2 = -\frac{1}{2}\frac{CV^2}{d} \tag{6}$$

Three configurations of capacitive actuators are used frequently. Apart from the parallel plate capacitor, both transverse comb drive and lateral comb drive devices are frequently. The configurations and related properties are discussed in the following.

Transverse comb drive

The configuration of TCD is shown in Fig. 2. The dark electrodes are stators where as the white fingers are movable. The displacement of the movable finger is perpendicular to the distance between electrodes. Namely, the displacement tends to decrease the distance between the movable finger with one fixed finger electrode while increasing the distance for another.

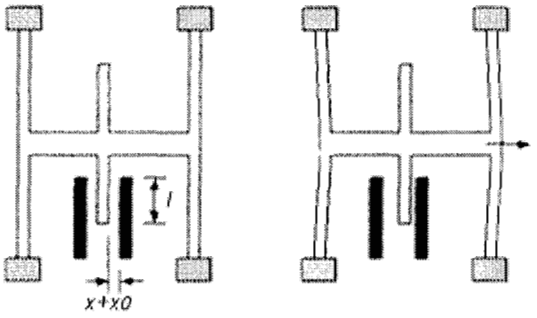

Fig. 2. Schematic diagram of transverse mode comb drive actuators.

The overall capacitance of the TCD is

$$C_{s1} = N(\frac{\varepsilon_0 lt}{x_0 + x} + C_f)$$
$$C_{s2} = N(\frac{\varepsilon_0 lt}{x_0 - x} + C_f) \tag{7}$$

where t is the thickness of the beams, and C_f is the fringe capacitance. The term N is the number of comb finger pairs within a TCD system. The subscript 1 represents the first set of electrode (located to the right hand side of the movable electrode) and the subscript 2 represents the second set of electrode (to the left). The capacitance at rest (x=0) is simply

$$C\big|_{x=0} = N(\frac{\varepsilon_0 lt}{x_0} + C_f) \tag{8}$$

At the equilibrium position, the force applied to the movable mechanism is

$$|F| = \frac{1}{2}\frac{N\varepsilon_0 lt}{x_0^2}V^2. \qquad (9)$$

When the shuttle is moved from its equilibrium position (x not equal to 0), the force is the balance of two components contributes by two sets of stators. Here, we assume the stators are biased to a voltage of V_0, and the potential of the moving shuttle is V_x. In consequence,

$$F = \frac{1}{2}\frac{C_0}{x_0}[(V_0 - V_x)^2 - (V_0 + V_x)^2] = \frac{2C_0V_0V_x}{x_0}. \qquad (10)$$

Lateral comb drive

Lateral comb drive has similar geometry as transverse comb drive. The moving fingers translate along the long axis of fingers. The system configuration is shown in Fig. 3 below.

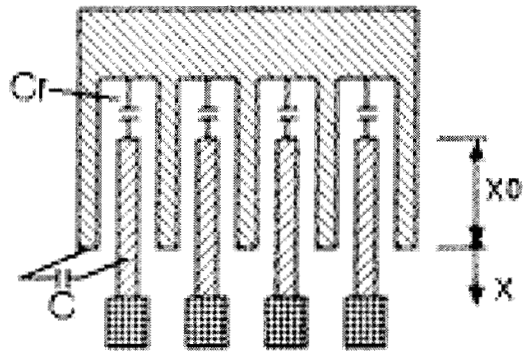

Fig. 3. Schematic diagram of lateral comb drive devices.

The relevant equations for the lateral comb drive are summarized in the following table.

Terms	Expression
Total capacitance	$C_{tot} = N[\frac{\varepsilon_0 t(x+x_0)}{d} + c_p]$
Gradient of capacitance	$\frac{\partial C}{\partial x} = N\frac{\varepsilon_0 t}{d}$
Force	$F\|_{x=0} = \frac{1}{2}\frac{N\varepsilon_0 t}{d}V^2$

Magnetic Actuation

A common component of these actuators is a thin-film structure plate that supports an electroplated Permalloy piece, which generates mechanical force and torque when it is placed within a magnetic field. These actuators are distinguished by the nature of their mechanical supports, which are based on

cantilever beams (Type-1 actuator, Fig. 4a) and torsion beams (Type-2 actuator, Fig. 4b). Both the structure plates and support beams are made of polycrystalline silicon thin films.

The mechanism of actuation is illustrated using the example of a Type-1 actuator (Fig 5a). Three terms, *L*, *W*, and *T*, represent the length, width, and thickness of the magnetic piece, respectively. The cantilever beam is *l* long, *w* wide, and *t* in thickness. When the external magnetic field is zero, the structural plate is parallel to the substrate plane (Fig. 5a). When an external magnetic field, H_{ext}, is applied normal to the plane of the structure plate, a magnetization vector, *M*, develops within the Permalloy piece and subsequently interacts with H_{ext} (Fig. 5b). The interaction creates a torque (M_{mag}) and a small force (*F*), acting at the free ends of the cantilever beams and causing these to bend (Fig. 5c).

An analysis of the quasi-static characteristics of these actuators is provided in the following two sections. The torque M_{mag} and force *F* due to magnetic interaction will first be analyzed. The overall displacement of the actuator is then derived.

When an external bias is applied, the Permalloy material is treated as having a fixed in-plane magnetization with its magnitude being equal to the saturation magnetization, M_s. Two force components are generated when the external magnetic field is applied. The magnitude of these two forces, F_1 (acting at the upper edge) and F_2 (acting at the lower edge) (Fig. 5b), are given by

$$F_1 = M_s \cdot W \cdot T \cdot H_1$$
$$F_2 = M_s \cdot W \cdot T \cdot H_2 \qquad (11)$$

where H_1 and H_2 are the magnetic field strengths at the top and bottom edges of the plate ($H_2 > H_1$ in the current configuration). The magnitudes of H_1 and H_2 are linearly dependent on the respective distance to the surface of the electromagnet core.

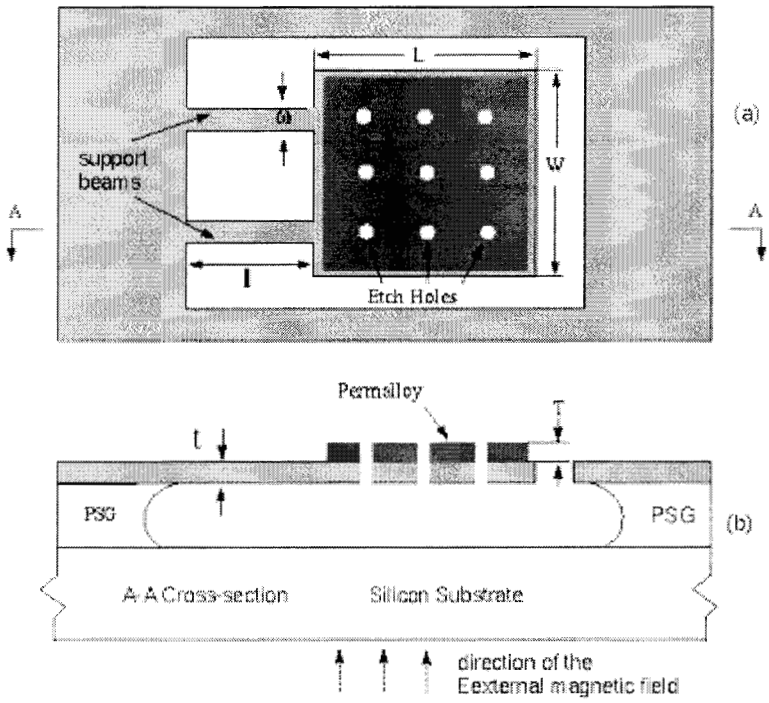

Fig. 4. Schematic of a Type-1 Permalloy magnetic actuator with two cantilever-beam supports. (a) Top view and (b) side view.

The structure plate, along with the Permalloy piece, has a thickness of $t+T$. Its moment of inertia, I, is proportional to $(t+T)^3$ and is much greater compared with that of the cantilever beam, which has a thickness of t. The structure plate, combined with the Permalloy piece, is thus considered as a rigid body. Based on this assumption, the force system is simplified by translating F_1 to coincide with F_2. The result is a counter-clockwise torque M_{mag} and a point force F acting on the bottom edge of the structural plate. These are expressed as

$$M_{mag} = F_1 L\cos\theta$$
$$F = F_2 - F_1 \qquad (12)$$

The torque always tends to minimize the overall energy in an actuator system by aligning the magnetization with the field lines of the external magnetic field.

Thermal Bimetallic Actuation

The scanning electron micrographs of fabricated actuators are shown in Fig. 6, with the measured deflection characteristics illustrated in Fig. 7. The theoretical analysis and measurement match well.

Fig. 8 shows a schematic of a typically bimetallic cantilever microactuator and defines the geometry. The length of the two layers combines in the sandwich like structure are assumed to be equal as this configuration provides the maximum force. Assuming that $\alpha_1<\alpha_2$, where a is the thermal expansion coefficient. The expression for the curvature is derived as:

$$\frac{1}{r} = \frac{6b_1b_2E_1E_2t_1t_2(t_1+t_2)(\alpha_2-\alpha_1)\Delta T}{(b_1E_1t_1^2)^2 + (b_2E_2t_2^2)^2 + 2b_1b_2E_1E_2t_1t_2(2t_1^2+3t_1t_2+2t_2^2)}. \qquad (13)$$

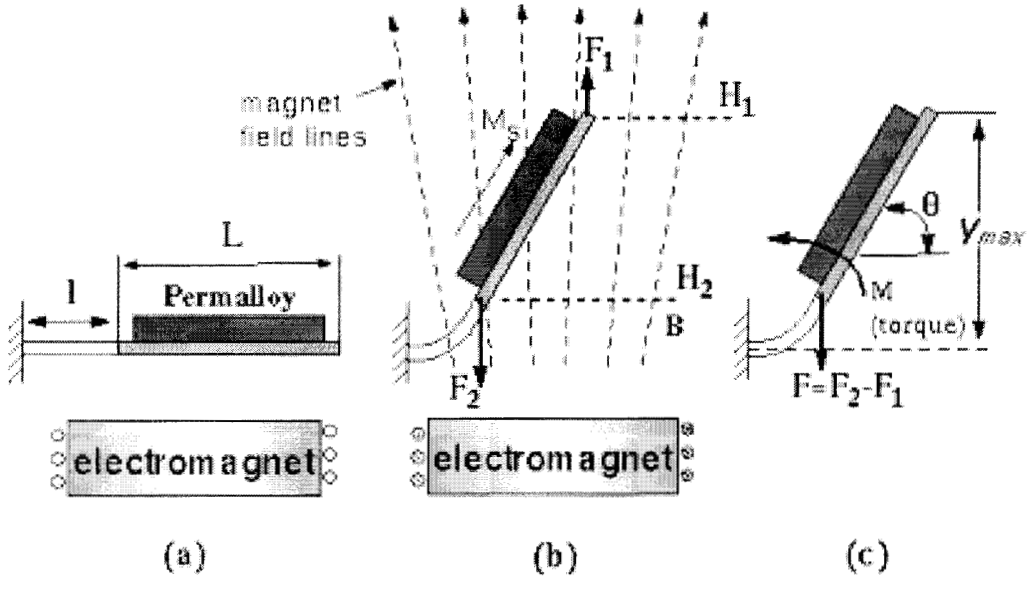

Fig. 5. Schematic illustration of the mechanism of Type-1 magnetic actuator biased using an external electromagnet. (a) Rest position of the actuator when $H_{ext}=0$; (b) out-of-plane actuation when $H_{ext} \neq 0$ is provided by an external electromagnet; F_1 and F_2 are the induced magnetic forces on the upper and lower edges of the plate; (c) a simplified force system (containing M_{mag} and F) acting at the free-ends of the cantilever beams.

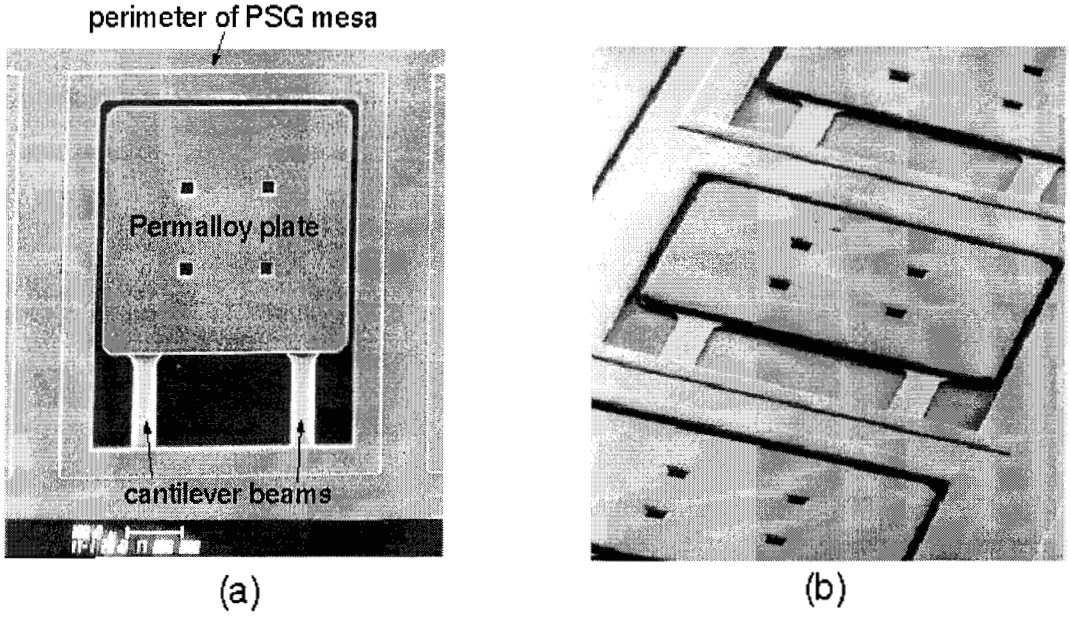

Fig. 6. SEM micrograph of (a) top view and (b) perspective view of a Type-1 actuator.

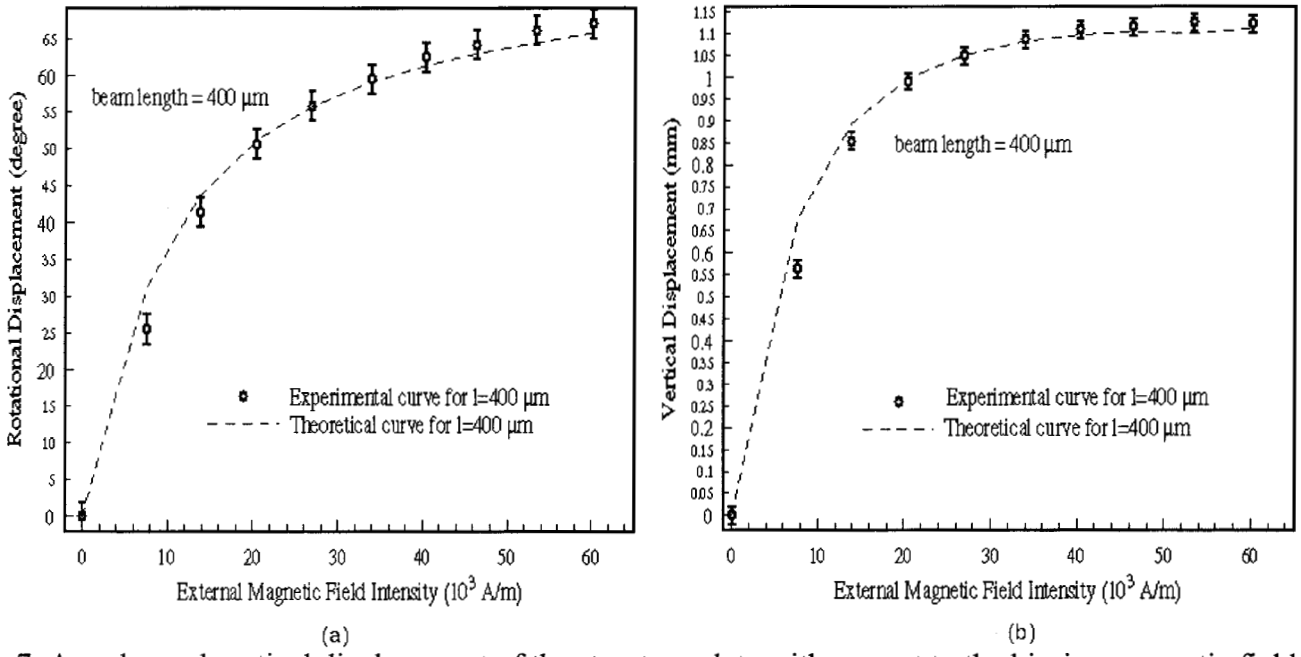

Fig. 7. Angular and vertical displacement of the structure plate with respect to the biasing magnetic field intensity H. (a) Theoretical and experimental rotation angle θ; (b) vertical deflection y_{max}. The size of the plate is 1x1mm^2, the beam length and width are 400 and 100 μm, respectively. The beam thickness is 1 μm.

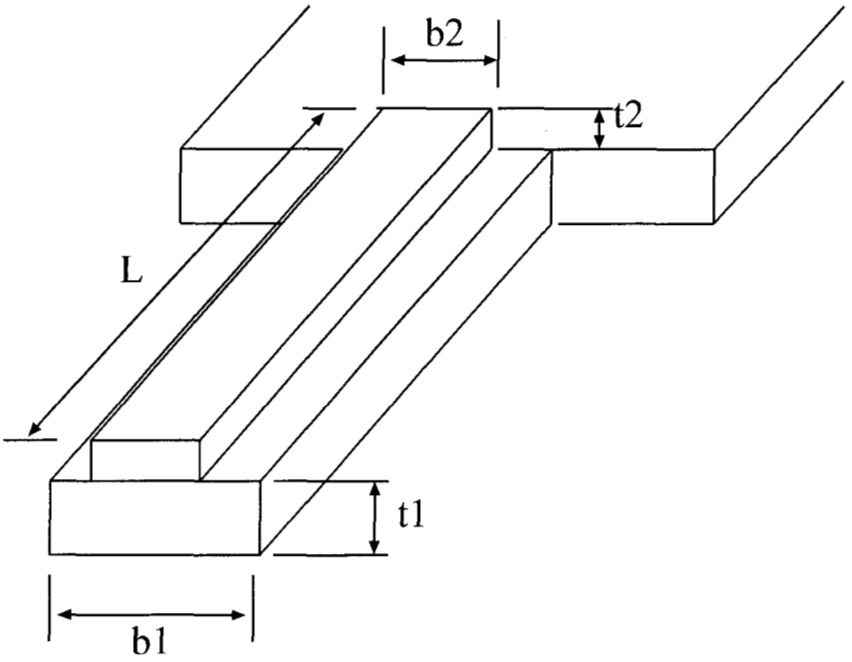

Fig. 8 Schematic diagram of the bimetallic stripe.

Piezoelectric Actuation

The charge produced by applied strain can be expressed in the following:

$$D = d\,T \tag{14}$$

where D is the electrical displacement on unit area and T is the stress. In the converse piezoelectric effect, the strain (S) and the electrical field (E) are related by the following relationship:

$$S = d\,E. \tag{15}$$

Both D and T are vectors while T and S being tensors. Units of components within the d matrix are either C/N (charge per newton) or m/V (strain per unit electric field, V/m).

The general relationship between strain (six components including surface normal strain and shear strain) and electric fields (three components including field components in x, y and z directions.) is typically summarized in vector form:

$$\begin{aligned} D_1 &= d_{11}T_1 + d_{12}T_2 + d_{12}T_3 + d_{14}T_4 + d_{15}T_5 + d_{16}T_6 \\ D_2 &= d_{21}T_1 + d_{22}T_2 + d_{23}T_3 + d_{24}T_4 + d_{25}T_5 + d_{26}T_6 \\ D_3 &= d_{31}T_1 + d_{32}T_2 + d_{33}T_3 + d_{34}T_4 + d_{35}T_5 + d_{36}T_6 \end{aligned} \tag{16}$$

where as the first digit in the subscript of d represent the direction of the electrical field (or displacement) and the second digit represent the direction of the strain that is involved. In many cased, materials have abbreviated [d] matrix such as:

$$\begin{pmatrix} 0 & 0 & 0 & 0 & d_{15} & 0 \\ 0 & 0 & 0 & d_{24} & 0 & 0 \\ d_{31} & d_{32} & d_{33} & 0 & 0 & 0 \end{pmatrix}$$

On the other hand, the relationship between strain and applied electric field (for piezo ceramic material) is expressed as

$$\begin{pmatrix} s1 \\ s2 \\ s3 \\ s4 \\ s5 \\ s6 \end{pmatrix} = \begin{pmatrix} 0 & 0 & d31 \\ 0 & 0 & d31 \\ 0 & 0 & d33 \\ 0 & d15 & 0 \\ d15 & 0 & 0 \\ 0 & 0 & 0 \end{pmatrix} \begin{pmatrix} E1 \\ E2 \\ E3 \end{pmatrix}$$

The most commonly used piezoelectric materials along with their properties are listed in the table below.

Material	Type	Form	Coefficient (pC/N)	Permitivity εr
quartz (x-cut)	Glass	Bulk	2.33	4
PVDF	Polymer	thin film	1.59	-
ZnO	Ceramic	Bulk	11.7	9
ZnO	Ceramic	Bulk	12.4	10.3
BaTiO3	Ceramic	Bulk	190	4,100
PZT (PbZrTiO3)	Ceramic	Bulk	370	300-3000
PZT	Ceramic	thin film	450 [11]	-

(Source for row 1 to. 6: (6))

III. DISCUSSIONS

Using existing microfabrication methods, large force and large displacement can not be readily achieved under the constraint of power consumption, volume, or voltage. Electrostatic actuation requires significant applied voltage for actuation. Magnetostatic and thermal bimetallic actuation use large power, for generating magnetic field and for providing temperature differentail, respectively. The achievable displacement of the piezoelectric material still is limited by the relatively low coupling coefficient. Electroactive materials with low driving voltage and large displacement is of critical important for advancing the technology of micro actuation and MEMS.

Generally, MEMS are fabricated primarily using silicon and related thin film materials (silicon nitride, polycrystalline silicon, etc.) Silicon, as a mechanical material, has a number of desired characteristics. For instance, the fracture stress of silicon is on the same order as that of steel while its specific mass is only approximately three times lower. In the past decade, a wide variety of microfabrication techniques have been developed for silicon materials, including bulk anisotropic etching, sacrificial surface micromachining, electroplating, reactive ion etching, among others. However, a major material problem associated with silicon is its low fracture strain, which is on the order of 0.1%. The fact that silicon can not tolerate large bending strain and significant impact seriously limits the possible applications. Moreover, silicon is also associated with high cost, where the basic material, silicon wafer, costs approximately $1 for each square inch of area. Polymers offer an

attractive basis for MEMS as a substrate as well as a construction material. Soft polymer materials that can be efficiently microfabricated at low cost, with exhibit desirable mechanical properties are highly desirable. Further, as the EAP technology evolves there may become a necessity to imbed MEMS into the EAP actuators to allow sensing, control, etc. Some of the characteristics that would benefit both the field of MEMS in general as well as the EAP actuation technology are:

- Polymer materials are elastic, can absorb impact energy and tolerate large degree of deformation.
- Polymer materials can be formed into three-dimensional structures using micro molding process as well as efficient high aspect ratio three-dimensional structures.
- The material is relatively inexpensive compared with silicon.

IV. ACKNOWLEDGEMENT

The Jet Propulsion Laboratory (JPL), California Institute of Technology, part of this research was carried out under a contract with National Aeronautics Space Agency (NASA) as part of the telerobotic program, funded by Code S and Dr. Chuck Weisbin is the Program Manager at JPL.

V. REFERENCES

1. A. Pisano, MEMS 2003 and beyond: a DARPA vision of the future of MEMS, *SPIE 6th Int. Symp. On Smart strcutures and materials*, Plenary presentation, 1999.
2. G.T.A. Kovacs, *Micromachined Transducers Sourcebook*, McGraw-Hill, 1998.
3. Hiroyuki Fujita, "A Decade of MEMS and Its Future, " *Proceedings of the Tenth Annual International workshop on MEMS (MEMS 97),* Nagoya, Japan.
4. J. Bryzek, K. Petersen and W. McCulley, "Micromachines on the March," *IEEE Spectrum, May* 1994.
5. M. Madou, *Fundamentals of microfabrication*, CRC Press, 1998.
6. J.W. Gardner, *Microsensors: Principles and applications*, Wiley, 1994.
7. M. Tabib-Azar, Integrated optics, microstructures, and sensors, Kluwar Academic Pub., 1995.S. Sze, Ed, Semiconductor sensors, Wiley Interscience, 1994.
8. W.H. Ko, Q. Qiang, and Y. Wang, Touch mode capacitive pressure sensors for industrial applications, *Solid state sensor and actuator workshop*, p. 244, 1996.
9. R. Service, Silicon chip find role as in vivo pharmacist, *Science*, 283 (5402), 1999.
10. D.H. Lewis, S.W. Janson, R.B. Cohen, E.K. Antonsson, Digital micropropulsion, *Proc. Int. Conf. on Micro electromechanical systems*, p. 517, 1999.
11. W. Hackenberger, *et. al.* (with Penn State University), Piezoelectric thick films for ultrasonic transducer arrays, *Proceedings, ISHM 96.*